

Phase Asymmetry for Ultrasound Denoising Within Fractional Anisotropic Diffusion and Total Variation

Kun M., Bin Han, Bowen Fu, Bin Qin^{ID}, Member, IEEE

Abstract—We propose an ultrasound speckle filtering method for not only preserving various edge features but also filtering tissue-dependent complex speckle noises in ultrasound images. The key idea is to detect these various edges using a phase congruence-based edge significance measure called phase asymmetry (PAS), which is invariant to the intensity amplitude of edges and takes 0 in non-edge smooth regions and 1 at the idea step edge, while also taking intermediate values at slowly varying ramp edges. By leveraging the PAS metric in designing weighting coefficients to maintain a balance between fractional-order anisotropic diffusion and total variation (TV) filters in TV cost function, we propose a new fractional TV framework to not only achieve the best despeckling performance with ramp edge preservation but also reduce the staircase effect produced by integral-order filters. Then, we exploit the PAS metric in designing a new fractional-order diffusion coefficient to properly preserve low-contrast edges in diffusion filtering. Finally, different from fixed fractional-order diffusion filters, an adaptive fractional order is introduced based on the PAS metric to enhance various weak edges in the spatially transitional areas between objects. The proposed fractional TV model is minimized using the gradient descent method to obtain the final denoised image. The experimental results and real application of ultrasound breast image segmentation show that the proposed method outperforms other state-of-the-art ultrasound despeckling filters for both speckle reduction and feature preservation in terms of visual evaluation and quantitative indices. The best scores on feature similarity indices have achieved 0.867, 0.844 and 0.834 under three different levels of noise, while the best breast ultrasound segmentation accuracy in terms of the mean and median dice similarity coefficient are 96.25% and 96.15%, respectively.

Index Terms—Ultrasound despeckling, speckle noise, fractional-order diffusion filter, fractional-order TV filter, edge detection, phase congruency, phase asymmetry, image denoising.

Manuscript received March 13, 2019; revised October 16, 2019; accepted November 8, 2019. Date of publication November 19, 2019; date of current version January 23, 2020. This work was supported by National Natural Science Foundation of China under Grant 61271320, and the Ministry of Education, China under Grant J1210001. This work was also supported by the National Natural Science Foundation of China under Grant YG2014MS29, and the Training Program of Excellent Talents under Grant J1210001. This work was also supported by the National Natural Science Foundation of China under Grant ZH2018ZDA19. This work was supported by the National Natural Science Foundation of China under Grant 61271320. (Corresponding author: Binjie Qin.)
K. M., B. Han, B. Qin, and S. B. Fu are with the School of Information Science and Technology, Beijing University of Aeronautics and Astronautics, Beijing 100191, China (e-mail: qinbj@buaa.edu.cn).
B. Han, B. Fu, and D. R. Man are with the School of Information Science and Technology, Beijing University of Aeronautics and Astronautics, Beijing 100191, China (e-mail: hanbin@buaa.edu.cn).
B. Fu, B. Han, and D. R. Man are with the School of Information Science and Technology, Beijing University of Aeronautics and Astronautics, Beijing 100191, China (e-mail: fubowen@buaa.edu.cn).
R. T. O. is with the School of Information Science and Technology, Beijing University of Aeronautics and Astronautics, Beijing 100191, China (e-mail: rto@buaa.edu.cn).
DOI: 10.1109/TIP.2019.2953361

I. INTRODUCTION

CURRENT ultrasound images are often contaminated by speckle noise [1], [2] which is a complex noise [3], [4] that is not only correlated in space but also in intensity. This noise is often modeled as a multiplicative noise [5], [6]. In order to remove speckle noise, various methods have been proposed, such as non-local means [7], S-NLM [8], NLNet [9], and NLNet [10]. These methods are based on the idea of exploiting the self-similarity of ultrasound images. However, these methods are often computationally expensive. In this paper, we propose a new fractional-order TV model for ultrasound despeckling. The proposed model is based on the idea of leveraging the phase asymmetry (PAS) metric to design weighting coefficients for fractional-order anisotropic diffusion and total variation (TV) filters. The proposed model is minimized using the gradient descent method to obtain the final denoised image. The experimental results and real application of ultrasound breast image segmentation show that the proposed method outperforms other state-of-the-art ultrasound despeckling filters for both speckle reduction and feature preservation in terms of visual evaluation and quantitative indices. The best scores on feature similarity indices have achieved 0.867, 0.844 and 0.834 under three different levels of noise, while the best breast ultrasound segmentation accuracy in terms of the mean and median dice similarity coefficient are 96.25% and 96.15%, respectively.

[15] In [15] ... [16] ... [17] ... [18] ... [19] ... [20] ... [21] ... [22] ... [23] ... [24] ... [25] ... [26] ... [27] ... [28] ... [29] ... [30] ... [31] ... [32] ... [33] ... [34] ... [35] ... [36] ... [37] ... [38] ... [39] ... [40] ... [41] ... [42] ... [43] ... [44] ... [45] ... [46] ... [47] ... [48] ... [49] ... [50] ... [51] ... [52] ... [53] ... [54] ... [55] ... [56] ... [57] ... [58] ... [59] ... [60] ... [61] ... [62] ... [63] ... [64] ... [65] ... [66] ... [67] ... [68] ... [69] ... [70] ... [71] ... [72] ... [73] ... [74] ... [75] ... [76] ... [77] ... [78] ... [79] ... [80] ... [81] ... [82] ... [83] ... [84] ... [85] ... [86] ... [87] ... [88] ... [89] ... [90] ... [91] ... [92] ... [93] ... [94] ... [95] ... [96] ... [97] ... [98] ... [99] ... [100] ...

[29] ... [30] ... [31] ... [32] ... [33] ... [34] ... [35] ... [36] ... [37] ... [38] ... [39] ... [40] ... [41] ... [42] ... [43] ... [44] ... [45] ... [46] ... [47] ... [48] ... [49] ... [50] ... [51] ... [52] ... [53] ... [54] ... [55] ... [56] ... [57] ... [58] ... [59] ... [60] ... [61] ... [62] ... [63] ... [64] ... [65] ... [66] ... [67] ... [68] ... [69] ... [70] ... [71] ... [72] ... [73] ... [74] ... [75] ... [76] ... [77] ... [78] ... [79] ... [80] ... [81] ... [82] ... [83] ... [84] ... [85] ... [86] ... [87] ... [88] ... [89] ... [90] ... [91] ... [92] ... [93] ... [94] ... [95] ... [96] ... [97] ... [98] ... [99] ... [100] ...

Acronym

[Redacted text block]

[Redacted text block]

In [48] [50] (AM-FM) [51], [40] [52]. T [53] w r
 2D f n
 nR r.T n n fM
 : fM = (f, fR) = (f, r1*f, r2*f), w r fR
 R r n f, r1(x1, x2) n r2(x1, x2) r
 r r n n R r, wn w :

$$\begin{aligned} r_1(x_1, x_2) &= \frac{-x_1}{2\pi(x_1^2 + x_2^2)^{3/2}} \\ r_2(x_1, x_2) &= \frac{-x_2}{2\pi(x_1^2 + x_2^2)^{3/2}} \end{aligned} \quad (1)$$

S n n r n r n n w r n
 r n , n n n fM n
 w n , r r r b. T n n
 n fM n fM = (b*f, b*r1*f, b*r2*f) =
 (es, os), w r es n os n
 r r n r
 S r n n r b n r
 , es n os; w C, m
 n r, n C, m n n
 r n n n F, r r n [54]. In
 r n n, 2D r C, m n
 wn :

$$C(w) = n_c |w|^a \quad (-s |w|), a \geq 1 \quad (2)$$

w r w = (w1, w2) n, r r , n
 r n, nc = (pi*4^{a+1}*s^{2a+1} / Gamma(2a+1))^{1/2}, Gamma(.) n n,
 n a n w . W a = 1.58, n [39].
 T n n r n , r , K [44] ,
 , PAS r r n r . T r r ,
 w n n - PAS w :

$$PA = \sum_s \frac{[|os| - |es| - Ts]}{\sqrt{e_s^2 + o_s^2} + \varepsilon} \quad (3)$$

w r PA PAS r , epsilon n n
 n r, Ts n n r ,
 [.] r r n r n n , n s n
 r n C, m . S , s n n r n
 r n n n n r , n n r n s
 w r r n n n (r m r n)
 n n r , n n w n
 n .

F. 1 w n PAS r r n
 . W n n n n n n r
 n PAS s = 5 n s = 10 w r , r
 n . T , n r n PAS s = 20
 n s = 25 n n , r .
 T PAS s = 15 n n n w n
 , n r n n n r r n. T , w
 s = 15 n r , r , n .

F. 1. E PAS r r n . () T , r , n
 n; PAS : () s = 5, () s = 10, () s = 15,
 () s = 20, () s = 25.

PAS r n r r n n
 n . T PAS r r r 0 1, n 0
 (n n n n n) n n r n
 n n l (n n n n) r
 . In n r , n n r
 n n . A n r , PAS
 n r n r n r , w n n
 n . F r r r n , r n
 , PAS n r n l.

B. Fractional-Order Differential

T r n - r r r n r n n n -
 n n n r r r r n , r n n r -
 n [47]. F r , r r n n f(x) in L^2(R),
 r n - r r r r n n w :

$$D^\alpha f(x) = \frac{d^\alpha f(x)}{dx^\alpha} \quad (4)$$

w r alpha n n r n r. T F, r r r n r
 D^\alpha f(x) w :

$$\begin{aligned} D^\alpha f(x) &\stackrel{FT}{\leftrightarrow} (\hat{D}^\alpha f)(w) = (iw)^\alpha \hat{f}(w) \\ &= |w|^\alpha [i \theta^\alpha(w)] \hat{f}(w) \\ &= |w|^\alpha \left[\frac{\alpha \pi i}{2} \cdot n(w) \right] \hat{f}(w) \end{aligned} \quad (5)$$

w r w n, r r , n , n(.) n n r
 n n r r , n (iw)^\alpha = |w|^\alpha [alpha pi / 2 * n(w)]
 r , n n r n r n . A r -
 n r , n n , w n r w , r
 n r - r , n r r r n n r n
 w r n alpha, n F. 2. Fr F. 2,
 n n n w-r , n w 0 < w < 1,
 r n r n n n n n . N -
 r , n n w w > 1, r n r n
 n r n r , n n n
 w r n r r n r r alpha n r . T n
 n , n n n n n n - r , n
 , w r n - r r r r n n
 n n n n n n .
 D , n r n r , n r , r-
 n n . A r r n r n - r r , n

Fig. 2. The original image (left) and the filtered image (right) using the proposed method.

The proposed method is based on the fractional-order anisotropic diffusion (FOAD) and total variation (TV) regularization. The FOAD is defined as follows [46]:

$$D^\alpha f(x) \triangleq \lim_{h \rightarrow 0} \frac{1}{h^\alpha} \sum_{l=0}^{[\frac{d-c}{h}]} (-1)^l \binom{\alpha}{l} f(x-lh) \quad (6)$$

where $\alpha \in (0, 1]$, $c, d \in \mathbb{R}$, and $f(x)$ is the function to be filtered. The binomial coefficient $\binom{\alpha}{l}$ is defined as follows [55], [56]:

$$\binom{\alpha}{l} = \frac{\Gamma(\alpha+1)}{\Gamma(l+1)\Gamma(\alpha-l+1)} \quad (7)$$

where $\Gamma(n) = (n-1)!$ for $n \in \mathbb{N}$.

C. Fractional-Order AD Filter and Fractional-Order TV Filter

The fractional-order AD filter is defined as follows [22]:

$$\frac{\partial u}{\partial t} = \text{div} [c(|\nabla u|) \cdot \nabla u], \quad (8)$$

where div is the divergence operator, $c(\cdot)$ is the conductivity function, and ∇u is the gradient of u .

... λ ... ;
 ... λ ...
 ... Tw ...
 ... In ...
 ... PSNR ...
 ... [60]. W ... $\lambda = 0.01$...
 ... R ...
 ... PAS ...
 ... w :

$$\begin{cases} \varphi = (PA - 1)^2 \\ \gamma = PA(2 - PA) \end{cases} \quad (15)$$

w r PA ...
 B ...
 w ... FAD ...
 W n PA ... 1, w ... FTV ...
 PA ... 1,
 FAD ...
 H w r, FAD ...
 w- n r ... T r-
 ... PAS ...
 ... T PAS ...
 w- n r ...
 n r . F r ... PAS ...
 ... W r ...
 (12). T ... w :

$$c(|\nabla^\alpha u|, PA) = 1 / \left[1 + \frac{|\nabla^\alpha u| \cdot (1 + 254 \cdot PA)}{k_1^2} \right] \quad (16)$$

w r $k_1 = k_0 e^{-0.05(n_{iter}-1)}$...
 H r, n_{iter} ...
 G n ...
 ... A r n ...
 ... S . II-B, w n ...
 ... PAS ...
 ... S ...
 ... r ...
 r ... [46] w :

$$\alpha = 1 + \frac{1}{2} (1 + PA^2) \quad (17)$$

w r PA ... PAS ... T ...
 $\alpha \in (1, 2)$. T ... PFDTV ...
 ... r ...
 ... r ...
 In ... PAS ...
 ... PAS ...

... n ... n ...
 ... A r n ... (17), ... PAS ...
 ... α ... T ...
 PFDTV ... w ...
 ... n ...
 ... w ...
 ... n ...

B. Numerical Solver

W r ... E r-L ... [61]
 ... (14). A ... u ...
 ... E(u) ...
 ... In ...
 u w ... W n ...
 ... 0, ...
 ... 0. T ...
 ... $\eta \in C^\infty(\Omega)$...
 ... e. D n ...

$$\begin{aligned} \Phi(e) &:= E(u + e\eta) \\ &= \int_{\Omega} [\varphi f(|\nabla^\alpha(u + e\eta)|) + \gamma |\nabla^\alpha(u + e\eta)|] dx dy \\ &\quad + \int_{\Omega} \left(\frac{\lambda}{2} |u + e\eta - u_0|^2 \right) dx dy \end{aligned} \quad (18)$$

W r ... $\Phi(e)$... w n :

$$\begin{aligned} \Phi'(e) &= \frac{d}{de} \Phi(e) \\ &= \varphi \int_{\Omega} \left(f'(|\nabla^\alpha(u + e\eta)|) \right. \\ &\quad \times \left. \frac{\nabla_x^\alpha(u + e\eta) \nabla_x^\alpha \eta + \nabla_y^\alpha(u + e\eta) \nabla_y^\alpha \eta}{\sqrt{(\nabla_x^\alpha(u + e\eta))^2 + (\nabla_y^\alpha(u + e\eta))^2}} \right) dx dy \\ &\quad + \gamma \int_{\Omega} \left(\frac{\nabla_x^\alpha(u + e\eta) \nabla_x^\alpha \eta + \nabla_y^\alpha(u + e\eta) \nabla_y^\alpha \eta}{\sqrt{(\nabla_x^\alpha(u + e\eta))^2 + (\nabla_y^\alpha(u + e\eta))^2}} \right) dx dy \\ &\quad + \lambda \int_{\Omega} (u + e\eta - u_0) \eta dx dy, \end{aligned} \quad (19)$$

L $e = 0$, n w ... w n :

$$\begin{aligned} \Phi'(0) &= \varphi \int_{\Omega} \left(c(|\nabla^\alpha u|^2, PA^2) (\nabla_x^\alpha u \nabla_x^\alpha \eta + \nabla_y^\alpha u \nabla_y^\alpha \eta) \right) dx dy \\ &\quad + \gamma \int_{\Omega} \frac{\nabla_x^\alpha u \nabla_x^\alpha \eta + \nabla_y^\alpha u \nabla_y^\alpha \eta}{|\nabla^\alpha u|} dx dy \\ &\quad + \lambda \int_{\Omega} (u - u_0) \eta dx dy \end{aligned} \quad (20)$$

w r $|\nabla^\alpha u| = \sqrt{(\nabla_x^\alpha u)^2 + (\nabla_y^\alpha u)^2}$. A r n ...
 ... r ... u, w n ...

$\Phi'(0) = 0$. Then, (20), we have

$$\nabla_x^\alpha u \nabla_x^\alpha \eta + \nabla_y^\alpha u \nabla_y^\alpha \eta = \left((\nabla_x^\alpha)^* \nabla_x^\alpha u + (\nabla_y^\alpha)^* \nabla_y^\alpha u \right) \eta \quad (21)$$

where $(\nabla_x^\alpha)^*$ and $(\nabla_y^\alpha)^*$ are the adjoint operators of ∇_x^α and ∇_y^α , respectively, as defined in [62]. By (20), we have

$$\begin{aligned} \Phi'(0) &= \varphi \int_{\Omega} c \left(|\nabla^\alpha u|^2, PA^2 \right) \left((\nabla_x^\alpha)^* \nabla_x^\alpha u + (\nabla_y^\alpha)^* \nabla_y^\alpha u \right) \eta \, dy \\ &\quad + \gamma \int_{\Omega} \frac{(\nabla_x^\alpha)^* \nabla_x^\alpha u + (\nabla_y^\alpha)^* \nabla_y^\alpha u}{|\nabla^\alpha u|} \eta \, dy \\ &\quad + \lambda \int_{\Omega} (u - u_0) \eta \, dy \end{aligned} \quad (22)$$

For $\eta \in C^\infty(\Omega)$, Euler-Lagrange equation is

$$\begin{aligned} \varphi c \left(|\nabla^\alpha u|^2, PA^2 \right) \left((\nabla_x^\alpha)^* \nabla_x^\alpha u + (\nabla_y^\alpha)^* \nabla_y^\alpha u \right) \\ + \gamma \frac{(\nabla_x^\alpha)^* \nabla_x^\alpha u + (\nabla_y^\alpha)^* \nabla_y^\alpha u}{|\nabla^\alpha u|} + \lambda (u - u_0) = 0 \end{aligned} \quad (23)$$

where $u \in E$, E is the function space defined by $E(u) = \int_{\Omega} |\nabla^\alpha u|^2 \, dy$, $\nabla E = 0$. Then, ∇E is

$$\begin{aligned} \nabla E = \varphi c \left(|\nabla^\alpha u|^2, PA^2 \right) \left((\nabla_x^\alpha)^* \nabla_x^\alpha u + (\nabla_y^\alpha)^* \nabla_y^\alpha u \right) \\ + \gamma \frac{(\nabla_x^\alpha)^* \nabla_x^\alpha u + (\nabla_y^\alpha)^* \nabla_y^\alpha u}{|\nabla^\alpha u|} + \lambda (u - u_0) \end{aligned} \quad (24)$$

Then, by [63], we have $u^{n+1} = u^n + \Delta t (-\nabla E)$, i.e., $u^{n+1} = u^n + \Delta t (-\nabla E)$. Finally, we have $u^{n+1} = u^n + \Delta t (-\nabla E)$.

C. Numerical Algorithm

Then, (24) can be written as G-L equation. We consider $u \in X \times Y$, where X and Y are the function spaces defined by $X = \{u \in L^2(\Omega) : \nabla_x^\alpha u \in L^2(\Omega)\}$ and $Y = \{u \in L^2(\Omega) : \nabla_y^\alpha u \in L^2(\Omega)\}$. Then, we have

$$\begin{cases} \nabla_x^\alpha u_{i,j} = \sum_{l=0}^j (-1)^l \binom{\alpha}{l} u_{i,j-l} \\ \nabla_y^\alpha u_{i,j} = \sum_{l=0}^i (-1)^l \binom{\alpha}{l} u_{i-l,j} \end{cases} \quad (25)$$

$$\begin{cases} (\nabla_x^\alpha)^* u_{i,j} = \sum_{l=0}^{Y-1-j} (-1)^l \binom{\alpha}{l} u_{i,j+l} \\ (\nabla_y^\alpha)^* u_{i,j} = \sum_{l=0}^{X-1-i} (-1)^l \binom{\alpha}{l} u_{i+l,j} \end{cases} \quad (26)$$

Algorithm 1 PFDTV F, r-Pr, r_n, D, F, r

Input:

TABLE II
COMPARISON OF THE PSNR, MSSIM AND FSIM VALUES AMONG DIFFERENT FILTERS



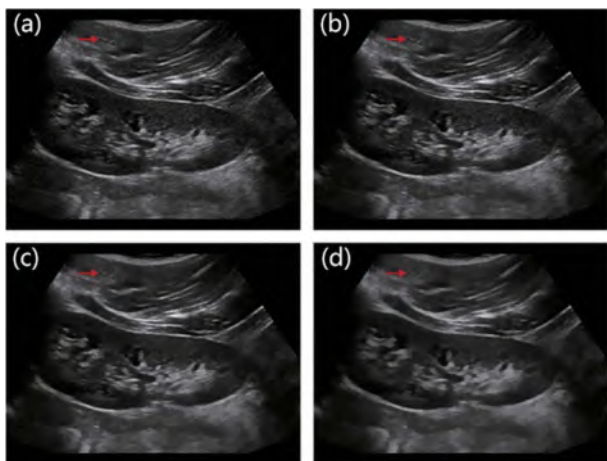


Fig. 4. Experimental results of the proposed method. (a) Original image, (b) $k_0 = 5$, (c) $k_0 = 20$, (d) $k_0 = 100$.

where w is the weight function, r is the original image, n is the noise, T is the total variation, $MSSIM$ is the mean structural similarity, $FSIM$ is the feature similarity, and $PFDTV$ is the proposed fractional total variation.

B. Clinical Image Experiment

The clinical image experiment is conducted on a set of 100 ultrasound images. The images are divided into two groups: training and testing. The training images are used to estimate the parameters of the proposed method. The testing images are used to evaluate the performance of the proposed method. The results are compared with other methods, including the total variation method, the fractional total variation method, and the proposed method. The proposed method shows superior performance in terms of speckle reduction and image quality. The parameters of the proposed method are $s = 0.5$, $k_0 = 5$, and $n_{iter} = 10$. The proposed method is implemented in MATLAB on a PC with 2.4 GHz CPU and 4 GB RAM.

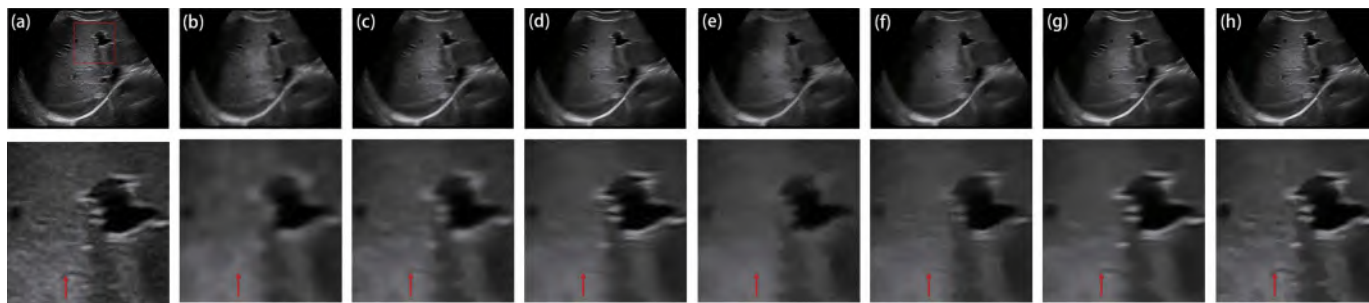


Fig. 6. Denoising results of the original image using SRAD, OBNLM, SBF, ADLG, NLLRF, and PFDTV. (a) Original image; (b) SRAD, (c) OBNLM, (d) SBF, (e) ADLG, (f) NLLRF, and (g) PFDTV.

Fig. 7. Denoising results of the original image using SRAD, OBNLM, SBF, ADLG, NLLRF, and PFDTV. (a) Original image; (b) SRAD, (c) OBNLM, (d) SBF, (e) ADLG, (f) NLLRF, and (g) PFDTV.

The results of the denoising process are shown in Fig. 7. The original image is shown in (a). The denoised images using SRAD, OBNLM, NLLRF, ADLG, SBF, and PFDTV are shown in (b) through (g), respectively. The results show that PFDTV (g) provides the most effective denoising performance, as it preserves the most structural information while removing the most noise. The zoomed-in regions in Fig. 7 show that PFDTV (g) maintains the most natural-looking texture and structure of the tissue, while the other methods (b-f) show varying degrees of blurring and loss of detail. The zoomed-in regions are shown in (b) through (g), respectively. The zoomed-in regions show that PFDTV (g) maintains the most natural-looking texture and structure of the tissue, while the other methods (b-f) show varying degrees of blurring and loss of detail.

rn . . . rn r n
rn n . r r n .
r wn w r w- nr
n () PFDTV.

SC n JS -
n n
r

J. E.
N RES
U ASOU
IS
10
9
2011

In [2], the ACVA method is proposed. In [78], [79] the PFDTV method is proposed. In [35], [76], [80] the 3D method is proposed. In [7], [81] the HW method is proposed. In [82] the TV method is proposed. In [38], [39] the FAD method is proposed. In [39] the FTV method is proposed. In [38], [39] the FAD method is proposed. In [39] the FTV method is proposed.

ACKNOWLEDGMENT

This work was supported by the National Natural Science Foundation of China (Grant No. 81273078).

- [29] A. S. L., and H. M. P., An new method for image denoising. *Measurement*, vol. 140, pp. 572–581, Jan. 2019.
- [30] D. G., R. S. An, and B. T., Signal denoising method. *IET Image Process.*, vol. 9, no. 2, pp. 107–117, 2015.
- [31] Z. Q., L. Y., and W. L., An new method for image denoising. *Proc. BMVC*, 2011, pp. 73.
- [32] V. B. S. Pr., R. P., G. S., and K. P., A new method for image denoising. *IEEE Trans. Image Process.*, vol. 28, no. 12, pp. 6198–6210, Dec. 2019.
- [33] N. O., M. G., S. A., A. Br., B. N., and R. B., On image denoising. *IEEE Trans. Pattern Anal. Mach. Intell.*, vol. 41, no. 10, pp. 2892–2904, Oct. 2019. [10.1109/TPAMI.2019.2892134](https://doi.org/10.1109/TPAMI.2019.2892134).
- [34] R. C., R. S., L. M., and H. B., A new method for image denoising. *arXiv:1904.10235*. [Online]. Available: <https://arxiv.org/abs/1904.10235>
- [35] V. K., A. F., K. E., and J. A., Fast image denoising. *Int. J. Comput. Vis.*, vol. 86, no. 1, pp. 1–32, 2010.
- [36] H. T., S. F., and P. M., Kernel-based image denoising. *IEEE Trans. Image Process.*, vol. 16, no. 2, pp. 349–366, Feb. 2007.
- [37] B. Q., Z. S., Z. Z., J. Z., and Y. L., Signal denoising. *Appl. Soft Comput.*, vol. 46, pp. 851–867, Sep. 2016.
- [38] B. Q., Z. S., Z. F., Z. Z., Y. L., and J. B., Joint image denoising. *IEEE Access*, vol. 6, no. 1, pp. 330–343, 2018.
- [39] L. Z., W. W., J. Q., K.-H. W., K.-S. C., and P.-A. H., Fast image denoising. *Signal Process.*, vol. 134, pp. 275–284, Mar. 2017.
- [40] A. B., D. B., and Y. M., A new method for image denoising. *IEEE Trans. Inf. Technol. Biomed.*, vol. 15, no. 1, pp. 138–147, Jan. 2011.
- [41] M. C. M., J. R., D. C. B., and R. O., A new method for image denoising. *Nature*, vol. 324, no. 6049, pp. 250–253, Nov. 1986.
- [42] M. C. M., and R. A. O., Fast image denoising. *Pattern Recognit. Lett.*, vol. 6, no. 5, pp. 303–313, Dec. 1987.
- [43] M. M., P. R., and J. A. N., 2D+T image denoising. *Med. Image Anal.*, vol. 4, no. 1, pp. 21–30, 2000.
- [44] P. K., Image denoising. *J. Comput. Vis. Res.*, vol. 1, no. 3, pp. 1–26, 1999.
- [45] G.-Q. Z., W.-W. J., K.-L. L., and Y.-P. Z., A new method for image denoising. *IEEE Trans. Med. Imag.*, vol. 36, no. 6, pp. 1250–1262, Jun. 2017.
- [46] Q. Z., J. G., Z. W., and K. L., A new method for image denoising. *IEEE Trans. Geosci. Remote Sens.*, vol. 54, no. 4, pp. 1905–1917, Apr. 2016.
- [47] J. Y., L. T., S. Z., L. W., and M. A. S., Image denoising. *IEEE Access*, vol. 5, pp. 12275–12285, 2017.
- [48] V. M., P. R., and M. S. P., Method for AM-FM image denoising. *IEEE Trans. Image Process.*, vol. 19, no. 5, pp. 1138–1152, May 2010.
- [49] J. P. H., P. T., and A. C. B., AM-FM image denoising. *Handbook of Image and Video Processing*. Academic Press, 2005, pp. 377–395.
- [50] M. C., T. O., and V. P., A new method for image denoising.

[76] B. G., A. D., S. A. r., B. S. S., n A. S. r., *Inf. Fusion*, 55, 220-244, Mar. 2020.

[77] C. A. N. S. n N. D. A. M. r., *IEEE Trans. Image Process.*, 28, n. 1, 216-226, Jun. 2019.

[78] Y. J. n, X. J. n, n W. J. n, *J. Vis. Commun. Image Represent.*, 65, Dec. 2019, Ar. n. 102661, doi: 10.1016/j.vci.2019.102661.

[79] Y.-F. P. et al., *IEEE Trans. Image Process.*, 27, n. 3, 1214-1229, Mar. 2018.

[80] F. Z. et al., *Phys. Med. Biol.*, 58, n. 6, 1739, 2013.

[81] R. J. G. n S. n, R. C. n, n Y. C. E. r, D. m. n, *Proc. IEEE*, 10.1109/JPROC.2019.2932116.

[82] X. J., S. L., X. F. n, n L. Z. n, *Proc. IEEE Conf. Comput. Vis. Pattern Recognit.*, Jun. 2019, 6054-6063.



Bin Hu received M.S. from Tsinghua University in 1997, and M.D.-P.D. from Southern Jiaotong University, Shenzhen, China, in 2006. He is currently an associate professor and the director of the State Key Laboratory of Intelligent Perception and Visual Understanding, Peking University, China. He is also an associate professor and the director of the Shenzhen Research Institute of Artificial Intelligence and Robotics.



Baowei Fei received M.S. and P.D. degrees from Case Western Reserve University, Cleveland, OH, USA. He is currently an associate professor and the director of the Engineering Center for Smart and Tissue Ultrasound Technology, Rice University, TX, USA, where he is also an assistant professor. He is also an associate professor and the director of the Center for Smart and Tissue Ultrasound Technology.



Kunqiang Mei received B.S. degrees from Tsinghua University and Arden University, and M.S. degrees from Tsinghua University and Southern Jiaotong University, Shenzhen, China, in 2016 and 2019, respectively. He is currently an associate professor and the director of the State Key Laboratory of Intelligent Perception and Visual Understanding.



Binjie Qin (M'07) received M.S. degrees from Tsinghua University and Southern Jiaotong University, Shenzhen, China, in 1999, and P.D. degrees from Southern Jiaotong University, Shenzhen, China, in 2002. He was a Lecturer in the Department of Signal Processing, Southern Jiaotong University, from 2012 to 2013, where he was also the director of the Department of Signal Processing, University of Cambridge, U.K. He is currently an associate professor and the director of the Shenzhen Research Institute of Artificial Intelligence and Robotics.